J. Fluid Mech. (1997), *vol.* 335, *pp.* 29–55

Stability of wall-bounded shear layers in the presence of simulated distributed surface roughness

By J. M. FLORYAN

Department of Mechanical Engineering, The University of Western Ontario, London, Ontario, N6A 5B9, Canada

(Received 4 March 1996 and in revised form 10 October 1996)

Linear stability of wall-bounded shear layers modified by distributed suction has been considered. Wall suction was introduced in order to simulate distributed surface roughness. In all cases studied, i.e. Poiseuille and Couette flows and Blasius boundary layer, wall suction was able to induce a new type of instability characterized by the appearance of streamwise vortices. Results of calculations show that a linear model of suction-induced flow modifications provides a sufficiently accurate representation of the basic state. The effects of an arbitrary suction distribution can, therefore, be assessed by decomposing this distribution into Fourier series and carrying out stability analysis on a mode-by-mode basis, i.e. once and for ever.

1. Introduction

Understanding how surface roughness affects the laminar–turbulent transition process is one of the fundamental questions in fluid mechanics. Resolution of this problem is of considerable practical importance, particularly for laminar airfoils in aeronautical applications. The difficulties stem from the fact that various physical mechanisms may initiate the transition process, depending on the distribution, amplitude and geometry of the roughness, and depending on the flow conditions.

There are an infinite number of possible forms of roughness elements. A methodology for characterization of the roughness is required so that the forms of roughness can be classified, with each class subject to separate investigations. The (unviable) alternative is to study each rough surface separately. The related questions are: (i) what parameters should be used to characterize a particular geometry, and (ii) how to define equivalent geometries.

The existing literature (see review by Floryan 1993) deals roughly with three classes of shapes: (i) single isolated two-dimensional roughness, i.e. trip wire; (ii) single isolated three-dimensional roughness, i.e. grain of sand; and (iii) distributed roughness. The key feature of the flow in the first case is the presence of separated wall-wakes. The main feature induced by a three-dimensional roughness element is a horseshoe vortex which extends in the downstream direction in the form of trailing vortices. There is no single feature that can be associated with distributed surface roughness.

Generally speaking, the presence of roughness favours transition in the sense that under otherwise identical conditions, transition occurs at a lower Reynolds number on a rough wall than on a smooth wall. If the roughness height is sufficiently small, it has no effect on the transition process; the corresponding walls are considered to be hydraulically smooth. A frequently used criterion is that the roughness Reynolds number $Re_k = U_k k/\nu < 25$ (Morkovin 1990), where k is the roughness height, U_k is the undisturbed velocity at height k and ν the kinematic viscosity. If the roughness height

is large, transition occurs immediately at the roughness element (i.e. tripping of flows). For moderate roughness height, transition occurs at a certain distance downstream from the location of the roughness, with this distance decreasing with an increase of the roughness height. Experimental investigations provide a phenomenological description of this process in the form of correlations between the height of the roughness, the flow conditions and the critical Reynolds number for certain classes of geometrical forms of the roughness (Schlichting 1979; Tani 1961). The range of applicability of these correlations is not certain because they are based on limited experimental data and have been determined for, in essence, artificially created roughness forms. These correlations, nevertheless, form the basis of all roughness sensitive designs.

The laminar–turbulent transition process in the case of smooth walls begins, typically, with instability in the form of linearly growing two-dimensional Tollmien–Schlichting waves followed by secondary instabilities and appearance of three-dimensional effects (Herbert 1988). Satisfactory transition prediction criteria can be obtained in such situations with the e^N method. Mechanisms promoting transition in the presence of surface roughness represent bypasses to the above scenario and lead to failure of the e^N method. These mechanisms, which strongly depend on the geometry of the roughness, are not known in the case of distributed surface roughness. Some of them have been identified in the case of a single roughness element, but understanding is insufficient to formulate quantitative correlations (Morkovin 1990). If a more rational basis for design correlations is to be established, the relevant mechanisms need to be identified and quantified.

The main objective of the present study is to elucidate the character of the laminar–turbulent transition process in the presence of distributed surface roughness. This problem is troublesome because the lack of any standardization of the roughness shape and distribution makes comparisons between various experiments (Kendall 1981; Reshotko & Leventhal 1981; Reshotko 1984; Corke, Bar Sever & Morkovin 1986) nearly impossible. The experiments indicate, nevertheless, that when the roughness is operative the departure from the laminar state is explosive (Reshotko 1984) with the underlying cause not being known (Morkovin 1990).

Doenhoff & Braslow (1961) describe early experiments with different models of surface roughness. Feindt (1957) used sand grains of different sizes and concluded that for $Re_r = Uk/\nu < 120$ the roughness has no influence and the transition takes place at the same location as on the smooth surface. Here k denotes the grain size, U stands for the velocity of the oncoming flow and ν denotes the kinematic viscosity.

Reshotko & Leventhal (1981) found that distributed roughness in the form of sand paper thickens the boundary layer and moves the essentially undeformed Blasius profile outward. The important growth of disturbances occurs in frequencies lower than those for which Tollmien–Schlichting waves are unstable. The amplification seems to be driven by the local wake profile at the crest of distributed roughness elements (Reshotko 1984). These observations contradict earlier theoretical investigations of Lessen & Gangwani (1976) and Singh & Lumley (1971) based on the premise that it is the distortion of the mean flow by the roughness that enhances instability.

Tadjfar *et al.* (1985) created distributed roughness using arrays of spheres attached to an otherwise smooth surface and measured velocity distribution between individual spheres. They have found no evidence of Tollmien–Schlichting waves. The results of their measurements suggest that the mechanism of transition is similar to the case of an isolated three-dimensional roughness element, i.e. it is driven by the horseshoe and hairpin vortices generated by the roughness element. The contribution of the downstream element should thus increase the strength of the upstream-generated

vortices towards eventual transition. Results of a direct numerical simulation of flow in the same geometry (i.e. flat surface with a regular array of spheres) suggest that the instability begins as the fluid in the wake behind a sphere becomes unstable and moves (De Anna 1993). The disturbances grow while being carried downstream above the next sphere (where the mean flow has an inflection point). The most amplified disturbance eventually reaches the wake behind the next sphere and induces a global response at a frequency governed by the streamwise spacing between the spheres.

Corke *et al*. (1986) carried out experiments using sand paper to represent distributed roughness. They reported (i) that it is the low-inertia fluid in the valleys between the grains that responds to free-stream disturbances, (ii) once Tollmien–Schlichting waves appear, they grow faster (although the reason is unknown) as compared to the smooth-wall case, and (iii) there is evidence of roughness-induced three-dimensionalization of the wave fronts leading to earlier secondary instabilities.

As evidenced by the above discussion, the distributed roughness is represented in controlled experiments by grains with various sizes and distribution (sand paper, arrays of spheres, etc.). It is not certain whether such models are equivalent to real wall roughness, which may be a result of manufacturing processes using, for example, different surface finishing techniques, degradation of the material (corrosion), debris deposition (flies, environmental pollution, etc.), icing or other causes.

Theoretical analysis of the effects of distributed surface roughness faces the same problem as experiments, i.e. how to realistically model all possible geometrical forms of the roughness. Floryan (1993) suggested using spectral and fractal models. In the former case, the rough wall can be represented in terms of Fourier series and, if the amplitude of the roughness is small in some sense, each mode can be considered separately. This leads to an analysis of flow over a wavy wall and possible interactions among various modes of wall waviness. The latter case, i.e. fractal models of boundary shapes, is very intriguing because it is possible to parameterize seemingly complicated shapes using just one parameter.

In the present analysis we shall use spectral models. In order to eliminate uncertainties associated with modelling of boundary conditions on an irregular boundary, we shall simulate roughness using fixed wall suction with a zero net mass flux. While the equivalence between such a simulated roughness and the actual one remains to be proven (Floryan 1990), the mechanisms governing the transition process are expected to be qualitatively similar, as evidenced by the discussion given at the end of this paper. The (arbitrary) wall suction will be decomposed into the Fourier series and the analysis will focus on a single mode only, with its wavenumber and the amplitude being the parameters. Such a simple model problem allows us to test a hypothesis that analysis of the effects of surface modifications on the mode-by-mode basis is physically meaningful. One should note that if the amplitude of the surface modifications is small enough, a one-mode (linear) model accurately describes the associated flow modifications. This offers two possibilities. In the first one, the (linear) flow modifications are strong enough to affect the flow evolution in a meaningful way (i.e. induce an instability) and this means that a fully rational analysis of the effects of distributed roughness is possible. In the second one, the (linear) modifications are too weak and the wall is equivalent to a hydraulically smooth wall. This means that the surface modifications have to induce a nonlinear distortion of the velocity field before they can affect the flow in a significant way. If this is the case, then each particular roughness distribution may have to be studied separately. We shall demonstrate in this paper that, at least for the suction-modified flow, the former is true.

Problem formulation and analysis will be described using Poiseuille flow as a

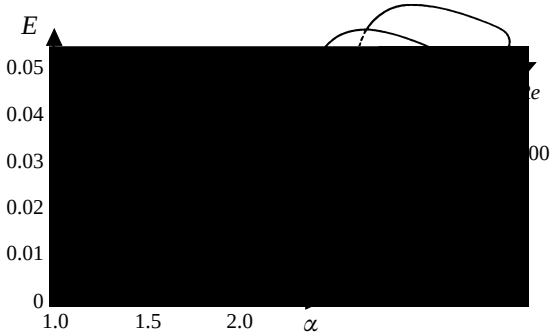

FIGURE 1. Neutral stability surface for the two-dimensional Tollmien–Schlichting waves for plane Poiseuille flow (Herbert 1977). E denotes energy of disturbances.

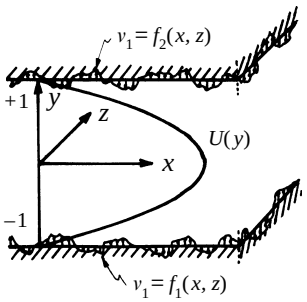

FIGURE 2. Plane Poiseuille flow with distributed wall suction.

reference case. The same analysis will then be applied to Couette flow and the Blasius boundary layer. It is useful to begin with a brief discussion of our reference case, i.e. the transition process in the Poiseuille flow under ideal conditions (no surface roughness). Linear critical Reynolds and wavenumbers have been determined to be $Re_L = 5772.22$ and $\alpha_L = 1.02055$ (Orszag 1971). The neutral surface for finite-amplitude two-dimensional disturbances is shown in figure 1 and its intersection with the plane corresponding to zero disturbance energy level defines the linear neutral stability curve. It can be seen that for $Re < Re_L$ disturbances will not grow unless their initial amplitude is sufficiently large. If this condition is met (bottom of the neutral surface in figure 1), disturbances will grow until they reach the top of the neutral surface which, therefore, defines stationary, two-dimensional equilibrium (saturation) states. Critical conditions for the nonlinear growth are $Re_{NL} \approx 2700$ and $\alpha_{NL} \approx 1.31$ (Herbert 1977). It may not be possible to reach such asymptotic states because the flow may suffer earlier secondary, three-dimensional instabilities (Herbert 1988). We shall refer to the diagram shown in figure 1 as describing the spectrum of natural response of the flow.

There are two ways of qualitatively describing the transition process in the presence of surface roughness. In the classical one (see, for example, Schlichting 1979) it is argued that the existence of roughness elements gives rise to additional disturbances in the laminar stream which have to be added to those already coming from the environment. If disturbances created by the roughness are bigger that those coming from the environment, we should expect that a lower degree of amplification will be sufficient to effect the transition. It is also possible to induce the instability at $Re < Re_L$ owing to its subcritical character. These arguments rely on the spectrum of natural response and point out the fact that depending on the initial energy level of the

disturbances, we may reach the saturation state more or less rapidly. One should note that if this is the only possible transition scenario, then surface roughness should not be able to induce instability at wavenumbers outside the natural spectrum at any Re and at $Re < Re_{NL}$ for any wavenumber.

Another way of looking at the problem, which is adopted here, is to determine the form of the flow in the presence of (simulated) surface roughness and then to investigate the stability characteristics of this flow. The spectrum of natural response is not required for interpretation of the results and it may play no role in the description of the evolution of the flow since this is not a Poiseuille flow any more. Indeed, our results demonstrate the correctness of this approach, i.e. they document the existence of a completely new instability mechanism induced purely by the surface flow modifications and completely unrelated to the spectrum of natural response.

The presentation of our results is organized as follows. Section 2 describes the new, roughness-modified flow, §3 describes linear stability analysis of the flow, §4 discusses numerical results and in §5, we give a short summary of our main conclusions.

2. Channel flow with wall suction/blowing

In this section, we shall consider modification of the Poiseuille flow due to the presence of fixed suction at the walls.

2.1. *Reference flow*

Consider plane Poiseuille flow confined between rigid walls at $y = \pm 1$ and extending to infinity in the horizontal directions x, z (figure 2). In the absence of wall suction, the undisturbed fluid motion is described by

$$\left.\begin{aligned} \overline{\nu_0}(\bar{x}, t) = (u_0, w_0, \nu_0) = (1-y^2, 0, 0), \\ p_0(\bar{x}, t) = -2x/Re, \end{aligned}\right\} \tag{2.1}$$

where the fluid is directed towards the positive x-axis and the Reynolds number, Re, is based on the half-channel height and the maximum x-velocity. This flow is driven by a constant mean pressure gradient.

2.2. *Flow modifications*

At the upper and lower walls apply suction in the form:

$$\nu_1(x, z, -1) = f_1(x, z), \quad \nu_1(x, z, 1) = f_2(x, z), \tag{2.2}$$

where both f_1 and f_2 are Fourier transformable and carry no net mass flux over a suitably chosen interval in x, z. For the purposes of problem formulation, we shall confine our attention to a particular Fourier mode in the suction distribution, i.e.

$$\nu_1(x, z, -1) = \nu_1(x, z, +1) = S\cos(\alpha x) = \tfrac{1}{2}S\,\mathrm{e}^{\mathrm{i}\alpha x} + \text{c.c.} \tag{2.3}$$

This mode simulates a two-dimensional periodic wall roughness with the same wavenumber α and amplitude S at the upper and lower walls. In the above, S is real and c.c. stands for the complex conjugate.

The flow may be represented as:

$$\left.\begin{aligned} \bar{\nu}(\bar{x}, t) = \overline{\nu_0}(\bar{x}, t) + \overline{\nu_1}(\bar{x}, t) = [u_0(y), 0, 0] + [u_1(x, y), 0, \nu_1(x, y)], \\ p(\bar{x}, t) = p_0(x) + p_1(x, y), \end{aligned}\right\} \tag{2.4}$$

where $\overline{\nu_1}, p_1$ are velocity and pressure modifications due to the presence of wall suction. Substitution of the above representation of the flow quantities into the two-

dimensional Navier–Stokes and continuity equations results in the following form of the governing equations:

$$u_0\frac{\partial u_1}{\partial x}+u_1\frac{\partial u_1}{\partial x}+v_1\frac{\mathrm{d}u_0}{\mathrm{d}y}+v_1\frac{\partial u_1}{\partial y}=-\frac{\partial p_1}{\partial x}+\frac{1}{Re}\left(\frac{\partial^2 u_1}{\partial x^2}+\frac{\partial^2 u_1}{\partial y^2}\right), \tag{2.5a}$$

$$u_0\frac{\partial v_1}{\partial x}+u_1\frac{\partial v_1}{\partial x}+v_1\frac{\partial v_1}{\partial y}=-\frac{\partial p_1}{\partial y}+\frac{1}{Re}\left(\frac{\partial^2 v_1}{\partial x^2}+\frac{\partial^2 v_1}{\partial y^2}\right), \tag{2.5b}$$

$$\frac{\partial u_1}{\partial x}+\frac{\partial v_1}{\partial y}=0. \tag{2.5c}$$

The continuity equation is eliminated by defining stream function in the form:

$$u_1=\frac{\partial \Psi}{\partial y},\quad v_1=-\frac{\partial \Psi}{\partial x}. \tag{2.6}$$

The pressure is eliminated by taking $\partial/\partial y$ of (2.5a) and subtracting from it $\partial/\partial x$ of (2.5b). The resulting equation has the form:

$$\left(u_0\frac{\partial}{\partial x}+\frac{\partial \Psi}{\partial y}\frac{\partial}{\partial x}-\frac{\partial \Psi}{\partial x}\frac{\partial}{\partial y}\right)\nabla^2\Psi-\frac{\mathrm{d}^2u_0}{\partial y^2}\frac{\partial \Psi}{\partial x}=\frac{1}{Re}\nabla^2(\nabla^2\Psi), \tag{2.7}$$

where ∇^2 denotes nabla operator, and $\nabla^2\Psi$ is the modification of the spanwise component of the vorticity vector.

Since u_1, v_1, p_1 are periodic in x with period $\lambda_x=2\pi/\alpha$, the stream function can be represented as:

$$\Psi(x,y)=\sum_{n=-\infty}^{n=+\infty}\Phi_n(y)\,\mathrm{e}^{\mathrm{i}n\alpha x}, \tag{2.8}$$

where $\Phi_n=\Phi^*_{-n}$ in order for Ψ to be real. Here, star denotes complex conjugate. The functions $\Phi_n(y), n\geqslant 0$, are governed by a nonlinear system of ordinary differential equations in the form

$$\left[\mathrm{D}_n^2-\mathrm{i}n\alpha Re\left(u_0\mathrm{D}_n-\frac{\mathrm{d}^2u_0}{\mathrm{d}y^2}\right)\right]\Phi_n-\mathrm{i}\alpha Re\sum_{l=-\infty}^{l=+\infty}\left[l\frac{\mathrm{d}\Phi_{n-l}}{\mathrm{d}y}\mathrm{D}_l\Phi_l-(n-l)\Phi_{n-l}\mathrm{D}_l\frac{\mathrm{d}\Phi_l}{\mathrm{d}y}\right]=0, \tag{2.9}$$

where $\mathrm{D}_n=(\mathrm{d}^2/\mathrm{d}y^2)-n^2\alpha^2$. Equation (2.9) has been obtained by substituting (2.8) into (2.7) and separating Fourier components.

The boundary conditions corresponding to (2.3) have the form:

$$\frac{\mathrm{d}\Phi_n}{\mathrm{d}y}=0\quad(y=\pm1,\quad n\geqslant 0), \tag{2.10a}$$

$$\Phi_n=0\quad(y=\pm1,\quad n\geqslant 2), \tag{2.10b}$$

$$\Phi_1=\frac{\mathrm{i}S}{2\alpha}\quad(y=\pm1), \tag{2.10c}$$

$$\Phi_0=M_1\quad(y=+1), \tag{2.10d}$$

$$\Phi_0=M_2\quad(y=-1), \tag{2.10e}$$

where one of the constants M_1, M_2 is arbitrary and the other one has to be selected.

The reader may note that introduction of the wall suction increases resistance to the

flow. Thus, if the flow is driven by the same constant mean pressure gradient, the mass flow rate has to decrease. Alternatively, if one wants to maintain the same mass flow rate, the mean pressure gradient must increase. Selection of constants M_1, M_2 (or equivalent conditions) is relevant to which of the above cases one wants to consider. It is also possible to consider a case where both the mean pressure gradient and the mass flow rate change. We shall now discuss selection of these constants.

Equation for Φ_0 obtained from (2.9) with $n = 0$ has the form:

$$\frac{\mathrm{d}^4\Phi_0}{\mathrm{d}y^4} - \mathrm{i}\alpha\, Re \sum_{l=-\infty}^{l=+\infty} \left(l \frac{\mathrm{d}\Phi_{-l}}{\mathrm{d}y} \frac{\mathrm{d}^2\Phi_l}{\mathrm{d}y^2} + l\Phi_{-l} \frac{\mathrm{d}^3\Phi_l}{\mathrm{d}y^3} \right) = 0, \tag{2.11a}$$

and can be re-arranged as:

$$\frac{\mathrm{d}^4\Phi_0}{\mathrm{d}y^4} + 2\alpha\, Re\, \mathrm{Im}\left[\sum_{l=1}^{l=+\infty} l \frac{\mathrm{d}^2}{\mathrm{d}y^2} \left(\Phi_l^* \frac{\mathrm{d}\Phi_l}{\mathrm{d}y} \right) \right] = 0, \tag{2.11b}$$

where Im denotes imaginary part and star denotes complex conjugate. Single integration of (2.11*b*) gives:

$$\frac{\mathrm{d}^3\Phi_0}{\mathrm{d}y^3} + 2\alpha\, Re\, \mathrm{Im}\left[\sum_{l=1}^{l=+\infty} l \frac{\mathrm{d}}{\mathrm{d}y} \left(\Phi_l^* \frac{\mathrm{d}\Phi_l}{\mathrm{d}y} \right) \right] = A\, Re. \tag{2.12}$$

It can be shown that the constant of integration A describes the mean pressure gradient induced by the suction, i.e.

$$\left. \frac{\partial p_1}{\partial x} \right|_{n=0} = A. \tag{2.13}$$

This is done by taking (2.5*a*), substituting (2.6) and (2.8), extracting from the pressure field mode corresponding to $n = 0$ and rearranging the resulting expression.

Integration of (2.12) gives:

$$\frac{\mathrm{d}^2\Phi_0}{\mathrm{d}y^2} + 2\alpha\, Re\, \mathrm{Im}\left(\sum_{l=1}^{l=+\infty} l\Phi_l^* \frac{\mathrm{d}\Phi_l}{\mathrm{d}y} \right) = A\, Re\, y + B, \tag{2.14}$$

which, when combined with (2.10*a*), permits specification of the boundary conditions corresponding to the desired mean pressure gradient, i.e.

$$\left. \frac{\mathrm{d}^2\Phi_0}{\mathrm{d}y^2} \right|_{y=1} - \left. \frac{\mathrm{d}^2\Phi_0}{\mathrm{d}y^2} \right|_{y=-1} = 2A\, Re. \tag{2.15}$$

Another integration of (2.14) combined with (2.10*a*) results in:

$$\frac{\mathrm{d}\Phi_0}{\mathrm{d}y} = -2\alpha\, Re\, \mathrm{Im}\left(\int_{-1}^{y} \sum_{l=1}^{l=+\infty} l\Phi_l^* \frac{\mathrm{d}\Phi_l}{\mathrm{d}\zeta} \mathrm{d}\zeta \right) + \tfrac{1}{2} A\, Re\, (y^2 - 1) + B(y + 1), \tag{2.16}$$

where

$$B = \alpha\, Re\, \mathrm{Im}\left(\int_{-1}^{+1} \sum_{l=1}^{l=+\infty} l\Phi_l^* \frac{\mathrm{d}\Phi_l}{\mathrm{d}y} \mathrm{d}y \right).$$

One more integration gives an expression for the stream function corresponding to the mean flow modification, i.e.

$$\Phi_0 = -2\alpha\, Re\, \mathrm{Im}\left(\int_{-1}^{y} \int_{-1}^{\eta} \sum_{l=1}^{l=+\infty} l\Phi_l^* \frac{\mathrm{d}\Phi_l}{\mathrm{d}\zeta} \mathrm{d}\zeta\, \mathrm{d}\eta \right) + \tfrac{1}{2} A\, Re(\tfrac{1}{3} y^3 - y - \tfrac{2}{3}) + B(\tfrac{1}{2} y^2 + y + \tfrac{1}{2}) + D, \tag{2.17}$$

where D is an arbitrary constant. The change in the mass flux induced by the suction can now be evaluated as:

$$Q = \Phi_0(1) - \Phi_0(-1) = -2\alpha\, Re\, \mathrm{Im}\left(\int_{-1}^{+1}\int_{-1}^{y}\sum_{l=1}^{l=+\infty} l\Phi_l^* \frac{\mathrm{d}\Phi_l}{\mathrm{d}\zeta}\mathrm{d}\zeta\,\mathrm{d}y\right) - \tfrac{2}{3}A\, Re + 2B. \tag{2.18}$$

The boundary conditions (equivalent to (2.10d, e)) that lead to the desired mass flux modification Q can be specified as:

$$\Phi_0(-1) = 0, \quad \Phi_0(+1) = Q, \tag{2.19a, b}$$

where the former has been selected arbitrarily and the latter follows from (2.18). The corresponding mean pressure modification is given by (2.15).

The boundary conditions (equivalent to (2.10d, e)) that impose the desired mean pressure gradient modification have the form:

$$\left.\frac{\mathrm{d}^2\Phi_0}{\mathrm{d}y^2}\right|_{y=1} - \left.\frac{\mathrm{d}^2\Phi_0}{\mathrm{d}y^2}\right|_{y=-1} = 2A\, Re, \quad \Phi_0(-1) = 0, \tag{2.20a, b}$$

where the former is (2.15) re-written, and the latter has been selected arbitrarily. The corresponding mass flux modification is given by (2.18). One may note that condition (2.20a) is mixed, i.e. it involves values from both ends of the solution domain.

If the suction on both walls is symmetric in y, then all Φ_i have the symmetry property

$$\Phi_n(-y) = (-1)^{n+1}\,\Phi_n(y) \quad (n \geqslant 0), \tag{2.21}$$

and the boundary conditions become much simpler, i.e.

$$\left.\frac{\mathrm{d}^2\Phi_0}{\mathrm{d}y^2}\right|_{y=1} = -\left.\frac{\mathrm{d}^2\Phi_0}{\mathrm{d}y^2}\right|_{y=-1} = A\, Re, \tag{2.22}$$

in the case of a specified pressure gradient A, and

$$\Phi_0(1) = -\Phi_0(-1) = \tfrac{1}{2}Q, \tag{2.23}$$

in the case of a specified mass flux Q. The above conditions have to be supplemented by (2.10a–c) and by the symmetry conditions at $y = 0$.

If the suction is purely antisymmetric, then all Φ_n have the symmetry property

$$\Phi_n(-y) = -\Phi_n(y) \quad (n \geqslant 0), \tag{2.24}$$

the boundary conditions (2.22) and (2.23) remain unchanged, but the symmetry conditions at $y = 0$ change accordingly.

In the forthcoming discussion we shall confine our attention to the zero mass flux modification case ($Q = 0$), i.e. the same mass flow rate is maintained with and without the wall suction. All solutions have been obtained using general boundary conditions, and the symmetry properties have been used for verification of the accuracy of the calculations.

2.3. *Linear approximation*

When the amplitude S of the wall suction in (2.3) is small enough, all flow quantities can be represented as asymptotic (power series) expansions, with S being the expansion parameter. Substitution of these expansions into the (2.5)–(2.7) and retention of leading terms (terms $O(S)$) gives a linear description of the flow modifications due to

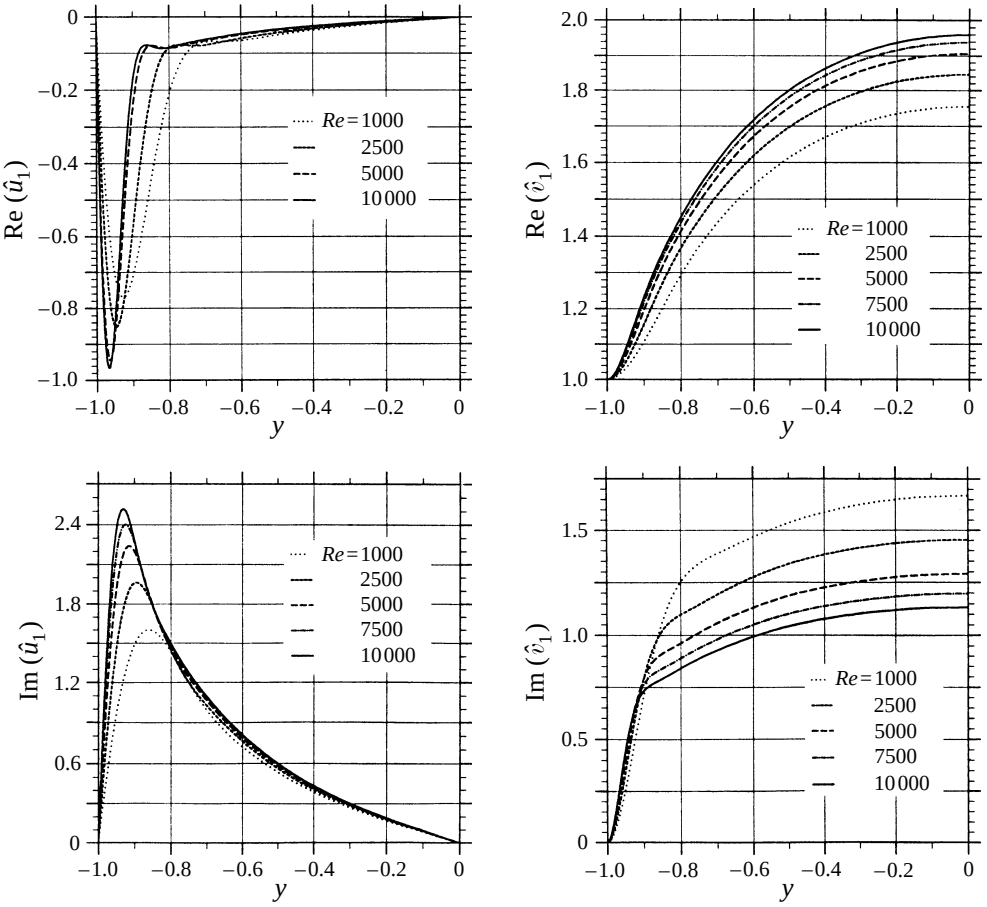

FIGURE 3. Modifications of the Poiseuille flow owing to the presence of wall suction as a function of the Reynolds number Re for $\alpha = 1.2$ obtained with a linear model (§2.3). Hats denote quantities normalized with $\frac{1}{2}S$ resulting in $v_1(\pm 1) = 1$.

the wall suction. This is equivalent to retaining only one term corresponding to $n = 1$ in (2.8). The relevant problem has the form:

$$\left\{\left(\frac{\mathrm{d}^2}{\mathrm{d}y^2}-\alpha^2\right)^2 - \mathrm{i}\alpha\, Re\left[u_0\left(\frac{\mathrm{d}^2}{\mathrm{d}y^2}-\alpha^2\right)-\frac{\mathrm{d}^2 u_0}{\mathrm{d}y^2}\right]\right\}\Phi_1 = 0, \tag{2.25}$$

$$\Phi_1 = \frac{\mathrm{i}S}{2\alpha}, \quad \frac{\mathrm{d}\Phi_1}{\mathrm{d}y} = 0 \quad \text{at} \quad y = \pm 1, \tag{2.26}$$

and has been solved using two different numerical methods. In the first one, a variable-step-size finite-difference discretization with deferred corrections was used (Pereyra 1979). The resulting algebraic system was solved by Gauss elimination. In the second one, the equations were discretized using a spectral collocation method based on Chebyshev polynomials. The resulting algebraic system for the expansion coefficients was solved using Gauss elimination.

Figures 3 and 4 illustrate velocity fields (normalized with a factor $\frac{1}{2}S$) for typical cases of interest. Results shown in figure 3 demonstrate that the character of the flow field changes very weakly as a function of the Reynolds number Re. Results displayed

in figure 4 demonstrate a rapid evolution of the flow field as a function of the wavenumber α. The qualitative differences can be shown explicitly by looking at the limits of $\alpha \to 0$ and $\alpha \to \infty$.

When $\alpha \to 0$, the system (2.25) and (2.26) can be solved analytically, following Floryan & Dallmann (1990). The unknown is represented as an asymptotic power series in terms of α, with the leading-order term being of order α^{-1}. The analysis gives leading-order approximation as:

$$\left.\begin{aligned} \Phi_1 &= S\left[\frac{\mathrm{i}}{2\alpha} - \tfrac{1}{24} Re\,(y^4 - 2y^2 + 1)\right], \\ u_1 &= S[-\tfrac{1}{6} Re\, y(y^2 - 1)]\, \mathrm{e}^{\mathrm{i}\alpha x} + \text{c.c.} \\ v_1 &= S[\tfrac{1}{2} + \tfrac{1}{24}\mathrm{i}\alpha\, Re\,(y^4 - 2y^2 + 1)]\, \mathrm{e}^{\mathrm{i}\alpha x} + \text{c.c.} \end{aligned}\right\} \tag{2.27}$$

Similarly, following Floryan & Dallmann (1990), one can work out an analytical solution for $\alpha \to \infty$. It consists of exponential boundary layers $O(\alpha)$ around both walls and a trivial solution in-between. The solution for the lower half of the channel has the form:

$$\left.\begin{aligned} \Phi_1 &= S\left[\frac{\mathrm{i}}{2\alpha}(1 + \alpha Y) + \frac{Re}{12\alpha} Y^2(1 + 3\alpha Y)\right] \mathrm{e}^{-\alpha Y} \\ u_1 &= S\left[-\tfrac{1}{2}\mathrm{i}\alpha Y + \frac{Re}{6\alpha} Y(1 + 3\alpha Y) + \tfrac{1}{4} Re\, Y^2 - \tfrac{1}{12} Re\, Y^2(1 + 3\alpha Y)\right] \mathrm{e}^{-\alpha Y + \mathrm{i}\alpha x} + \text{c.c.} \\ v_1 &= S\left[\tfrac{1}{2}(1 + \alpha Y) - \frac{\mathrm{i} Re}{12} Y^2(1 + 3\alpha Y)\right] \mathrm{e}^{-\alpha Y + \mathrm{i}\alpha x} + \text{c.c.} \end{aligned}\right\} \tag{2.28}$$

where $Y = y + 1$.

2.4. *Fourier truncation method*

Approximate solutions can be found by cutting the sum in (2.8) at a finite number N of terms and solving a coupled system of $N+1$ ordinary differential equations of type (2.9). Solutions for $N = 1, 2, 3$ were obtained using the algorithm described below.

The equations were discretized using variable-step-size finite-difference discretization with deferred corrections (Pereyra 1979) and the resulting algebraic system was solved using the Newton method. The solution strategy that was used in order to guarantee convergence of the iterative process consisted of obtaining at first a solution to the linear problem, then using this solution as an initial approximation of the solution for $N = 1$, then using solution for $N = 1$ as an initial guess for $N = 2$, and so on. For $N \geqslant 2$, a parameter continuation method had to be employed.

The success of the Fourier truncation method depends on the rate of convergence of the Fourier series. The relative importance of different modes can be assessed by calculating their energy. The energy E_n for mode n is defined as:

$$E_0 = \frac{1}{4}\int_{-1}^{1} \tilde{u}_0^2 \,\mathrm{d}y, \tag{2.29a}$$

$$E_n = \frac{1}{2}\int_{-1}^{1} |\bar{v}_{1n}|^2 \,\mathrm{d}y \quad (n \neq 0), \tag{2.29b}$$

where $\tilde{u}_0$ stands for the x-component of velocity vector corresponding to term $n = 0$ and $\bar{v}_{1n}$ stands for the velocity corresponding to term n in (2.8). Results shown in table 1 demonstrate that the series converge very rapidly for the small suction amplitudes S of interest in this analysis.

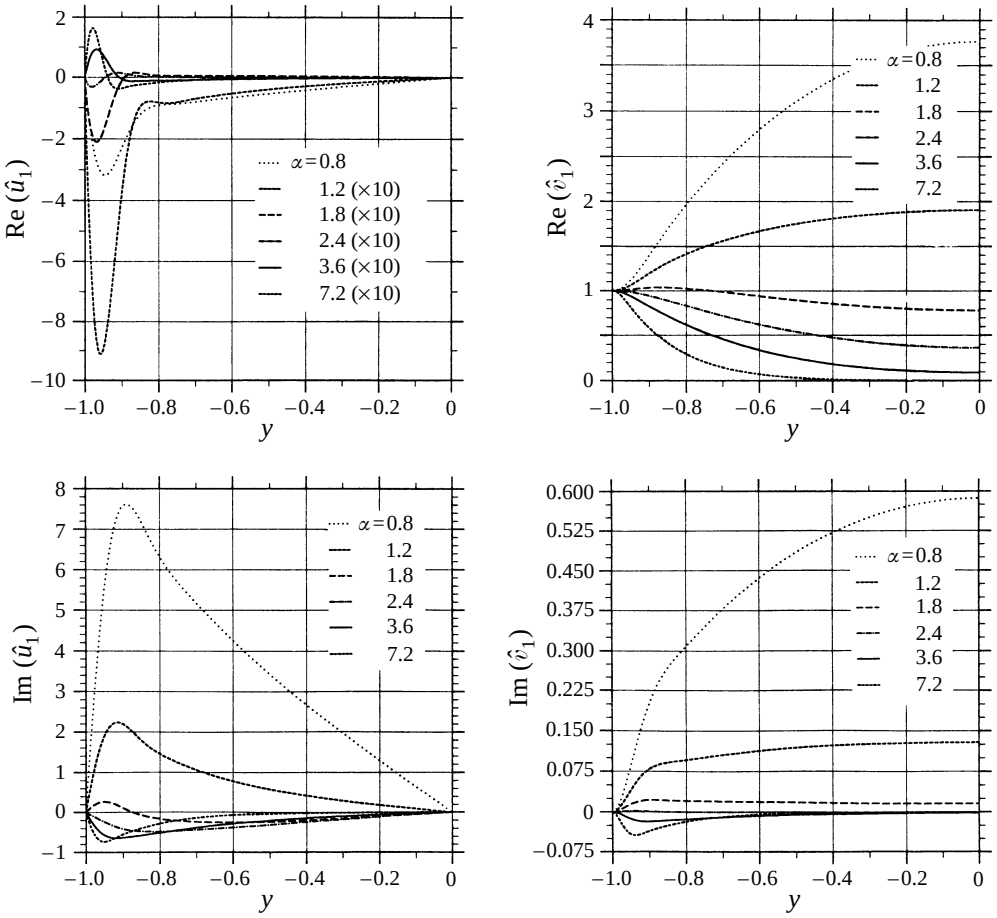

FIGURE 4. Modifications of the Poiseuille flow as a function of the wavenumber α for $Re = 5000$. Other conditions as in figure 3.

n	E_0	E_1	E_2	E_3
		$\alpha = 0.6$		
Linear	—	0.836×10^{-3}	—	—
1	0.914×10^{-4}	0.812×10^{-4}	—	—
2	0.102×10^{-3}	0.801×10^{-3}	0.358×10^{-5}	—
3	0.102×10^{-3}	0.800×10^{-3}	0.360×10^{-5}	0.130×10^{-6}
		$\alpha = 1.2$		
Linear	—	0.345×10^{-4}	—	—
1	0.163×10^{-5}	0.335×10^{-4}	—	—
2	0.171×10^{-5}	0.334×10^{-4}	0.236×10^{-7}	—
3	0.170×10^{-5}	0.334×10^{-4}	0.234×10^{-7}	0.313×10^{-9}
		$\alpha = 2.4$		
Linear	—	0.450×10^{-5}	—	—
1	0.233×10^{-9}	0.449×10^{-5}	—	—
2	0.243×10^{-9}	0.449×10^{-5}	0.914×10^{-10}	—
3	0.243×10^{-9}	0.449×10^{-5}	0.914×10^{-10}	0.203×10^{-12}

TABLE 1. Energy of the first four modes determined by truncating the Fourier series (2.8) at $N = n$, for $Re = 5000$, $S = 0.006$

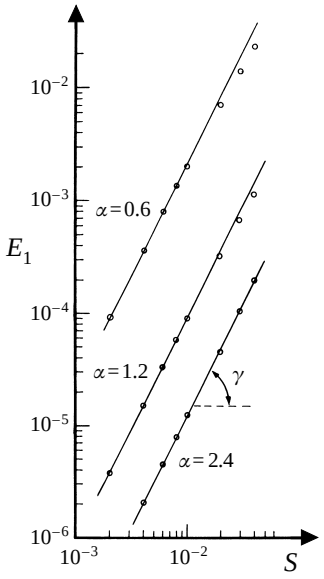

FIGURE 5. Energy E_1 of mode $n=1$ (equation (2.29b)) associated with the modifications of the Poiseuille flow owing to the presence of wall suction in the form (3.3) as a function of the suction amplitude S. Calculations have been carried out with $N=3$ (§2.4) *Note*: $\tan(\gamma)=2.0$.

Figure 5 illustrates variations of energy of mode $n=1$ as a function of suction amplitude S determined with $N=3$. It can be seen that mode interaction plays a negligible role for $S \leqslant 10^{-2}$. The reader may also note that nonlinear effects are more noticeable for $\alpha \to 0$.

3. Stability of channel flow with wall suction

This section describes the linear stability analysis of the Poiseuille flow modified by the fixed wall suction. The analysis refers to the Floquet theory owing to the periodic character of the flow modifications.

3.1. *Problem formulation*

The analysis begins with the governing equations in the form of vorticity transport and continuity equations

$$\frac{\partial \bar{\omega}}{\partial t} - (\bar{\omega}\cdot\boldsymbol{\nabla})\,\bar{v} + (\bar{v}\cdot\boldsymbol{\nabla})\,\bar{\omega} = \frac{1}{Re}\nabla^2\bar{\omega}, \tag{3.1a}$$

$$\boldsymbol{\nabla}\cdot\bar{v}=0, \quad \bar{\omega}=\boldsymbol{\nabla}\times\bar{v}. \tag{3.1b, c}$$

Unsteady, three-dimensional disturbances are superimposed on the mean part in the form

$$\bar{\omega}=\overline{\omega_2}(x,y)+\overline{\omega_3}(x,z,y,t), \quad \bar{v}=\overline{v_2}(x,y)+\overline{v_3}(x,z,y,t), \tag{3.2}$$

where subscripts 2 and 3 refer to the mean flow and the disturbance field, respectively. The assumed form (3.2) of the flow field is substituted into the governing equations (3.1), the mean part is subtracted and the equations are linearized. The resulting linear disturbance equations have the form

$$\frac{\partial \overline{\omega_3}}{\partial t} + (\overline{v_2}\cdot\boldsymbol{\nabla})\,\overline{\omega_3} - (\overline{\omega_3}\cdot\boldsymbol{\nabla})\,\overline{v_2} + (\overline{v_3}\cdot\boldsymbol{\nabla})\,\overline{\omega_2} - (\overline{\omega_2}\cdot\boldsymbol{\nabla})\,\overline{v_3} = \frac{1}{Re}\nabla_2\,\overline{\omega_3}, \tag{3.3a}$$

$$\boldsymbol{\nabla}\cdot\bar{v}_3=0, \quad \bar{\omega}_3=\boldsymbol{\nabla}\times\bar{v}_3. \tag{3.3b, c}$$

These equations can be written explicitly in the component form as follows

$$\frac{\partial \zeta_3}{\partial t}+u_2\frac{\partial \zeta_3}{\partial x}+v_2\frac{\partial \zeta_3}{\partial y}-\zeta_3\frac{\partial u_2}{\partial x}-\eta_3\frac{\partial u_2}{\partial y}-\phi_2\frac{\partial u_3}{\partial z}=\frac{1}{Re}\nabla^2\zeta_3, \tag{3.4a}$$

$$\frac{\partial \phi_3}{\partial t}+u_2\frac{\partial \phi_3}{\partial x}+v_2\frac{\partial \phi_3}{\partial y}+u_3\frac{\partial \phi_2}{\partial x}+v_3\frac{\partial \phi_2}{\partial y}-\phi_2\frac{\partial w_3}{\partial z}=\frac{1}{Re}\nabla^2\phi_3, \tag{3.4b}$$

$$\frac{\partial \eta_3}{\partial t}+u_2\frac{\partial \eta_3}{\partial x}+v_2\frac{\partial \eta_3}{\partial y}-\zeta_3\frac{\partial v_2}{\partial x}-\eta_3\frac{\partial v_2}{\partial y}-\phi_2\frac{\partial v_3}{\partial z}=\frac{1}{Re}\nabla^2\eta_3, \tag{3.4c}$$

$$\frac{\partial u_3}{\partial x}+\frac{\partial w_3}{\partial z}+\frac{\partial v_3}{\partial y}=0, \tag{3.4d}$$

where

$$\bar{v}_2=(u_2,0,v_2),\quad \bar{\omega}_2=(0,\phi_2,0),\quad \bar{v}_3=(u_3,w_3,v_3),\quad \bar{\omega}_3=(\zeta_3,\phi_3,\eta_3).$$

Only two of equations (3.4*a–c*) are independent.

The mean flow is assumed to have the form

$$\overline{v_2}(\bar{x},t)=[U_0(y),0,0]+\{[f_u(y),0,f_v(y)]\,\mathrm{e}^{\mathrm{i}\alpha x}+\text{c.c.}\}, \tag{3.5}$$

i.e. it is described by the first two modes ($N=0,1$) from (2.8). This description provides sufficiently accurate representation of the flow in the case of small amplitudes of suction being of interest here, as discussed in §2.4. When nonlinear effects are completely negligible, the mean flow can be represented as

$$\overline{v_2}(\bar{x},t)=[u_0(y),0,0]+\tfrac{1}{2}S\{[\hat{u}_1(y),0,\hat{v}_1(y)]\,\mathrm{e}^{\mathrm{i}\alpha x}+\text{c.c.}\}, \tag{3.6}$$

where $\hat{u}_1,\hat{v}_1$ are solutions of the linear problem (2.25) and (2.26) normalized so that $\hat{v}_1(\pm1)=1$. Distributions of $\hat{u}_1,\hat{v}_1$ for the parameters of interest are shown in figures 3 and 4.

The disturbance equations (3.4) have coefficients that are functions of x and y only (e.g. equation (3.5)). This permits separation of variables and representation of the t and z dependence of the solution in the form

$$\overline{v_3}(x,z,y,t)=\overline{u_3}(x,y)\,\mathrm{e}^{\mathrm{i}(\sigma t+\mu z)} \tag{3.7}$$

The exponent μ is real and accounts for the spanwise periodicity of the disturbance field. The exponent σ is assumed to be complex and its imaginary part describes the rate of growth of the disturbances while its real part describes the frequency of the disturbances.

Since the coefficients in (3.4) are periodic in x with periodicity $2\pi/\alpha$, $\bar{u}_3$ is written, following the Floquet theory (Coddington & Levinson 1965), as

$$\overline{u_3}(x,y)=\mathrm{e}^{\mathrm{i}\delta x}\,\overline{w_3}(x,y)=\mathrm{e}^{\mathrm{i}\delta x}\sum_{m=-\infty}^{m=+\infty}\overline{G_m}(y)\,\mathrm{e}^{\mathrm{i}m\alpha x}, \tag{3.8}$$

where $\bar{w}_3$ is periodic in x with the same periodicity $2\pi/\alpha$ and δ is referred to as the Floquet exponent. Our interest is in the temporal stability theory and thus δ is assumed to be real. One should note that $\bar{u}_3$ is a product of two functions periodic in x, one with a period $2\pi/\alpha$ and one with a period $2\pi/\delta$. This product is periodic only if δ/α is rational. For example, $\delta/\alpha=0.5$ results in $\bar{u}_3$ having period doubled as compared to $\bar{w}_3$. It is sufficient to consider $\delta\in[0,\alpha)$ since values of δ outside this interval can be accounted for, without loss of generality, by renumbering terms in the Fourier series in (3.8).

The final form of the disturbance velocity vector is written as

$$\overline{v_3}(x,z,y,t)=\sum_{m=-\infty}^{m=+\infty}[g_u^{(m)}(y),g_w^{(m)}(y),g_v^{(m)}(y)]\,\mathrm{e}^{\mathrm{i}[(\delta+m\alpha)x+\mu z+\sigma t]}, \tag{3.9}$$

where $g_u^{(m)}=g_u^{(-m)*}, g_w^{(m)}=g_w^{(-m)*}, g_v^{(m)}=g_v^{(-m)*}$ in order for $\overline{v_3}$ to be real. Here, star denotes complex conjugate.

Substitution of (3.5) and (3.9) into the disturbance equations (3.4) and separation of the Fourier components results, after rather lengthy algebra, in a system of linear ordinary differential equations governing $g_u^{(m)}, g_w^{(m)}, g_v^{(m)}, m\geqslant 0$, in the form

$$\begin{aligned}T^{(m)}(t_m g_w^{(m)}-\mu g_u^{(m)})+Re\,\mu \mathrm{D}U_0 g_v^{(m)}&=\mathrm{i}\,Re\,(N_u^{(m)}g_u^{(m-1)}+N_w^{(m)}g_w^{(m-1)}\\&\quad+N_v^{(m)}g_v^{(m-1)}+K_u^{(m)}g_u^{(m+1)}+K_w^{(m)}g_w^{(m+1)}+K_v^{(m)}g_v^{(m+1)}),\end{aligned} \tag{3.10a}$$

$$\begin{aligned}S^{(m)}g_v^{(m)}&=-Re\,(L_u^{(m)}g_u^{(m-1)}+L_w^{(m)}g_w^{(m-1)}+L_v^{(m)}g_v^{(m-1)}\\&\quad+M_u^{(m)}g_u^{(m+1)}+M_w^{(m)}g_w^{(m+1)}+M_v^{(m)}g_v^{(m+1)}),\end{aligned} \tag{3.10b}$$

$$\mathrm{i}t_m g_u^{(m)}+\mathrm{i}\mu g_w^{(m)}+\mathrm{D}g_v^{(m)}=0, \tag{3.10c}$$

where

$$\mathrm{D}=\frac{\mathrm{d}}{\mathrm{d}y},$$

$$\begin{gathered}t_m=\delta+m\alpha,\\ k_m^2=t_m^2+\mu^2,\\ T^{(m)}=\mathrm{D}^2-k_m^2-\mathrm{i}\,Re(t_m U_o+\sigma),\\ S^{(m)}=(\mathrm{D}^2-k_m^2)^2-\mathrm{i}\,Re(t_m U_o+\sigma)(\mathrm{D}^2-k_m^2)+\mathrm{i}\,Re\,t_m\mathrm{D}^2U_o,\\ N_u^{(m)}=-\mu t_m f_u+\mathrm{i}\mu f_v\mathrm{D},\\ N_w^{(m)}=(t_m^2-\alpha t_m)f_u-\mathrm{i}t_m f_v\mathrm{D},\\ N_v^{(m)}=\mathrm{i}\mu\mathrm{D}f_u,\\ K_u^{(m)}=\mu(-t_m f_u^*+\mathrm{i}f_v^*\mathrm{D}),\\ K_w^{(m)}=(t_m^2+\alpha t_m)f_u^*-\mathrm{i}t_m f_v^*\mathrm{D},\\ K_v^{(m)}=\mathrm{i}\mu\mathrm{D}f_u^*,\\ L_u^{(m)}=-t_m^2\mathrm{D}f_u+\mathrm{i}\alpha k_m^2 f_v+t_m(-t_m f_u+\mathrm{i}\mathrm{D}f_v)\mathrm{D}+\mathrm{i}t_m f_v\mathrm{D}^2,\\ L_w^{(m)}=\mu[-t_m\mathrm{D}f_u+\alpha\mathrm{D}f_u+(-t_m f_u+\alpha f_u+\mathrm{i}\mathrm{D}f_v)\mathrm{D}+\mathrm{i}f_v\mathrm{D}^2],\\ L_v^{(m)}=\mathrm{i}t_m\mathrm{D}^2f_u+k_m^2\mathrm{D}f_v+\mathrm{i}t_{m-1}k_m^2 f_u+(\mathrm{i}t_m\mathrm{D}f_u+k_m^2 f_v)\mathrm{D},\\ M_u^{(m)}=-t_m^2\mathrm{D}f_u^*-\mathrm{i}\alpha k_m^2 f_v^*+t_m(-t_m f_u^*+\mathrm{i}\mathrm{D}f_u^*)\mathrm{D}+\mathrm{i}t_m f_v^*\mathrm{D}^2,\\ M_w^{(m)}=\mu[-t_m\mathrm{D}f_u^*-\alpha\mathrm{D}f_u^*+(-t_m f_u^*-\alpha f_u^*+\mathrm{i}\mathrm{D}f_v^*)\mathrm{D}+\mathrm{i}f_v^*\mathrm{D}^2],\\ M_v^{(m)}=\mathrm{i}t_m\mathrm{D}^2f_u^*+k_m^2\mathrm{D}f_v^*+\mathrm{i}t_{m+1}k_m^2 f_u^*+(\mathrm{i}t_m\mathrm{D}f_u^*+k_m^2 f_v^*)\mathrm{D},\end{gathered}$$

and star denotes complex conjugate. Equation (3.10*a*) results directly from (3.4*c*), (3.10*c*) follows from (3.4*d*), and (3.10*b*) is obtained by multiplying (3.4*a*) by $\mathrm{i}\mu$ and subtracting from it (3.4*b*) multiplied by $\mathrm{i}t_m$. The above form of the equations has been simplified by taking advantage of the continuity equation.

Effects of the wall suction are contained in the terms on the right-hand side of (3.10*a–b*). In their absence, all modes from the Fourier series (3.9) decouple and equation (3.10) describe the classical three-dimensional instability of the ideal Poiseuille flow. The coupling due to the suction involves only three consecutive terms from the Fourier series.

	Number of modes M		
	1	2	3
Number of Chebyshev polynomials			
(*a*) 41	-0.4994×10^{-2}	-0.4963×10^{-2}	-0.4963×10^{-2}
51	-0.4994×10^{-2}	-0.4963×10^{-2}	-0.4963×10^{-2}
(*b*) 41	-0.4992×10^{-2}	-0.4961×10^{-2}	-0.4961×10^{-2}
51	-0.4992×10^{-2}	-0.4961×10^{-2}	-0.4961×10^{-2}

TABLE 2. Amplification $\mathrm{Im}(\sigma)$ of suction-induced disturbances. (*a*) Poiseuille flow. $Re = 5000$, $S = 0.006$, $\alpha = 1.8$, $\mu = 2.0$. Linear model of suction-induced flow modifications. (*b*) Suction-induced flow modifications described by the first two modes $n = 0, 1$ in (2.8). All other parameters as in (*a*).

Equations (3.10) together with homogeneous boundary conditions may have a non-trivial solution only for a certain combination of parameters δ, σ and μ. The required dispersion relation has to be determined numerically.

3.2. *Numerical solution*

The problem to be solved is described by an infinite set of coupled linear homogeneous ordinary differential equation (3.10) with homogeneous boundary conditions. Approximate solutions can be found by truncating the sum in (3.9) after a finite number M of terms and solving the eigenvalue problem for the two-point boundary-value problem for a system of $2M+1$ differential equations of type (3.10). The success of this approach depends on the rate of convergence of the Fourier series. Various tests, that have been carried out, show that for the values of suction amplitude S of interest in this study, the eigenvalues can be determined with accuracy no worse than 0.1% with $M = 1$ (see table 2) when $\alpha > 0.5$ and $M = 2$ when $\alpha < 0.5$. All results presented here have been obtained according to this rule.

Various tests have been carried out in order to assess the influence of the nonlinear distortion of the mean flow induced by the presence of wall suction on the stability characteristics of the complete flow (see (3.5)–(3.6)). It has been determined that for the magnitudes of the suction amplitude S considered in this study, effects of mean flow distortion, i.e. the term corresponding to $n = 0$ in (2.8), are negligible (see table 2). This is in agreement with conclusions discussed in §2.4. Thus, all results reported here have been obtained with the mean flow represented by (3.6). This conclusion is important in the sense that it shows that it is possible to replace an arbitrary suction distribution (2.2) by its Fourier decomposition and then carry out a linear stability analysis on the mode-by-mode basis. This makes the problem of arbitrary surface roughness distribution tractable. The above statement is obviously true provided that the roughness amplitude is sufficiently small. The discussion given in the next section shows that, in the case of wall suction, a suction amplitude S small enough to permit a mode-by-mode analysis is big enough to induce an instability.

The differential equations were discretized by employing a spectral collocation method based on Chebyshev polynomials (Casalis 1991). Accurate solutions can be obtained even with a relatively small number of collocation points, typically 40–50 in the present study (see table 2). The discretization was general in the sense that no special symmetry properties of the solution were assumed. Such symmetries, if present, were used for the verification of the accuracy of the numerical procedure.

The algebraic problem resulting from the discretization of the differential equations has a non-trivial solution only if the determinant of the matrix of coefficients becomes

zero. This was the condition used for identification of the eigenvalues. The eigenvalues σ, δ and μ involve four real quantities and only two of them can be calculated. Thus, in the calculations, two eigenvalues would be selected and the remaining two would be evaluated using a classical Newton–Raphson search procedure. A reasonable guess for the unknown eigenvalues is essential for the convergence of the search routine.

4. Discussion of results

We consider temporal stability theory, i.e. the exponent δ in (3.9) is assumed to be real. Exponent μ is real and accounts for the spanwise periodicity of the disturbance field. Exponent σ is complex and its imaginary part describes the rate of growth of the disturbances.

4.1. *Poiseuille flow with identical suction at both walls*

As a first case we shall consider the flow field that is modified by surface suction in the form (2.3), i.e. the suction is periodic in the streamwise direction with the period $2\pi/\alpha$ and it is the same at the upper and lower walls. The reader may recall that the ideal Poiseuille flow (i.e. in the absence of any surface modifications) becomes linearly unstable at $Re_L = 5772.22$ and that the critical disturbance has the form of a two-dimensional wave travelling in the streamwise direction.

Results of the present analysis show that the presence of the wall suction leads to the appearance of growing disturbances at Reynolds number $Re < Re_L$. The disturbances have the form of streamwise vortices, i.e. the dominant mode corresponds to $m = 0$ in (3.9). No subharmonics have been found, i.e. $\delta = 0$ in (3.9), which is in agreement with direct numerical simulations of Floryan, Yamamoto & Murase (1992). The disturbances are fixed with respect to the wall and do not propagate, i.e. $\mathrm{Re}(\sigma) = 0$ in (3.9). A whole band of the spanwise wavenumbers μ is amplified and the width of this band increases with an increase of both the suction amplitude S as well as the flow Reynolds number Re (see figures 6 and 7). Disturbances with $\mu \approx 2.0$ appear to have the largest amplification rates. The suction with the wavenumber $\alpha \approx 1.8$ appears to be the most dangerous in the sense that it induces disturbances with the highest amplification rates. The critical Reynolds number decreases with an increase of the suction amplitude S (see figures 6 and 7). The form of the disturbances is such that it leads to a rapid three-dimensionalization of the flow field.

The suction-induced instability identified above represents the initial stage of a new bypass route to transition, as shown by direct numerical simulation of Floryan *et al.* (1992). Flow evolution is driven by a different mechanism to the one that gives rise to the classical TS disturbances (Tollmien–Schlichting travelling waves). It can arise at $Re < Re_{NL}$ (see figure 1) and its occurrence is not related to the subharmonic character of the TS-instability.

Results presented in figures 8 and 9 permit making comparisons between the TS-waves and the disturbances induced by the wall suction. The amplification curves shown correspond to the two-dimensional TS-waves with the same wavelength as the wall suction. The wavenumber $\alpha = 1.8$, which corresponds approximately to the most amplified suction-induced-disturbances (see figures 6 and 7), has been selected for the comparison purposes. It can be seen that the TS-waves are slightly stabilized by the wall suction when $Re < 7500$ and that an increase of the suction amplitude S decreases their growth rates (figure 8). At $Re > 7500$ this trend is reversed. The overall changes of the growth rates as a function of the suction amplitude S are rather small, as illustrated by the results displayed in figure 9. The same trend has been identified in the

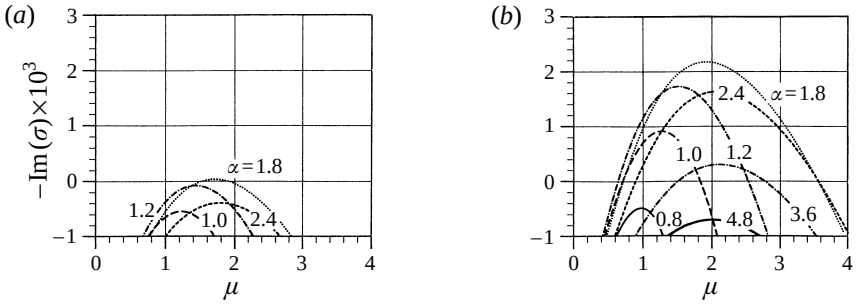

FIGURE 6. Amplification rate $-\mathrm{Im}(\sigma)$ as a function of the spanwise wavenumber μ for the suction-induced-disturbances in the Poiseuille flow with $Re = 3000$. The flow is modified by wall suction in the form (2.3) with the amplitude $S = 0.004$ in (a) and $S = 0.006$ in (b).

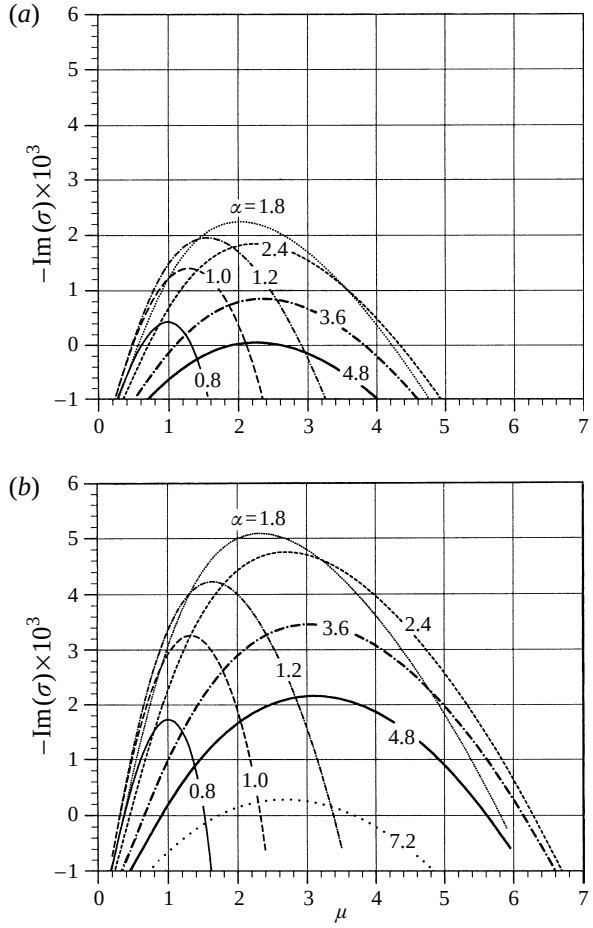

FIGURE 7. Same as figure 6. $Re = 5000$. (a) $S = 0.004$; (b) $S = 0.006$.

case of three-dimensional (oblique) TS-waves (not shown), i.e. they are also very little affected by the presence of wall suction.

Figures 8 and 9 contain information about the suction-induced-disturbances induced by the wall suction of the same wavelength as the TS-waves discussed above.

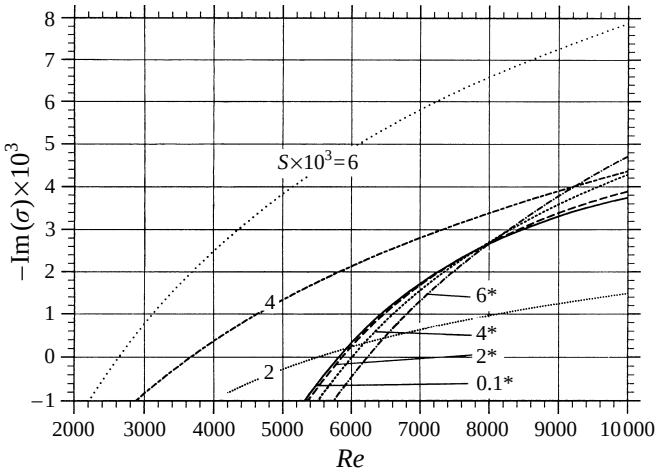

FIGURE 8. Amplification rate $-\mathrm{Im}(\sigma)$ as a function of the Reynolds number Re for the Poiseuille flow for the two-dimensional TS-waves and the suction-induced-disturbances (with $\mu = 2.0$) for various values of the suction amplitude S for $\alpha = 1.8$. Asterisks denote TS-waves.

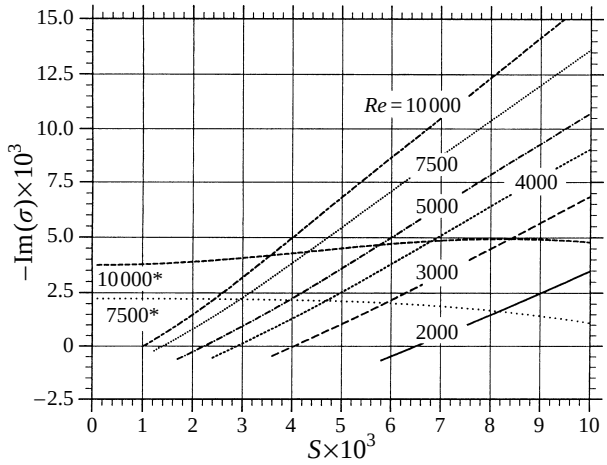

FIGURE 9. Amplification rate $-\mathrm{Im}(\sigma)$ as a function of the suction amplitude S for the Poiseuille flow for the two-dimensional TS-waves and the suction-induced-disturbances (with $\mu = 2.0$) for $\alpha = 1.8$ and various values of the Reynolds number Re. Asterisks denote TS-waves.

It can be seen in figure 8 that these disturbances can become unstable earlier than the TS-waves, their critical Reynolds number can be lowered by increasing the suction amplitude S, their growth rates are approximately of the same order of magnitude as growth rates of the TS-waves and these growth rates increase with an increase of the Reynolds number Re, similar to the case of the TS-waves. Figure 9 illustrates effects of the suction amplitude S. It can be seen that an increase of S leads to an almost linear increase of the amplification rates of the suction-induced disturbances (while the growth rates practically do not change for the TS-waves). Figure 9 also illustrates the fact that given a particular value of the Reynolds number Re, it is always possible (in the range of parameters studied) to find a suction amplitude S that gives rise to the vortex-like disturbances.

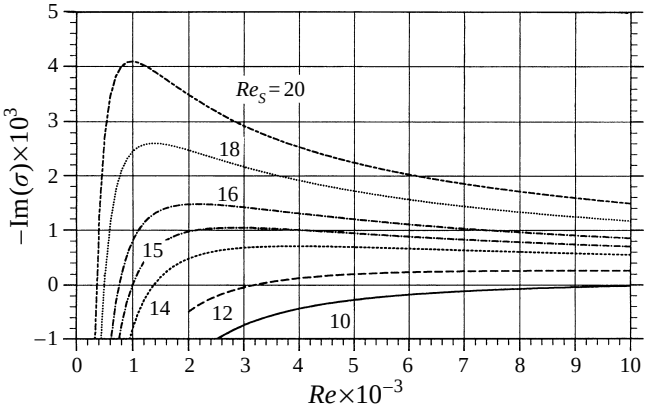

FIGURE 10. Amplification rate $-\mathrm{Im}(\sigma)$ as a function of the Reynolds number Re for the Poiseuille flow for various values of the suction Reynolds number Re_s with $\alpha = 1.8$, $\mu = 2.0$.

Presence of streamwise vortices results in uplifting of a low-momentum fluid away from the walls and creation of a highly distorted streamwise velocity profile that is a function of both the streamwise and the spanwise coordinates. Such profiles are subject to very strong secondary instabilities (Yu & Liu 1991) which may lead to a rapid transition to turbulence. The above scenario is the most likely (bypass) route to turbulence when Poiseuille flow is modified by wall suction, in view of the results given in figures 6–9.

Since the presence of streamwise vortices is a strong harbinger of transition to turbulence, one is interested in the maximum suction amplitude that the flow can accommodate without inducing such vortices. This information has already been given in figures 6–9, however, the results can be better interpreted by using suction Reynolds number $Re_s = S\,Re$, rather than the suction amplitude S, as a measure of the strength of the wall suction.

Re_s uses suction amplitude S as the velocity scale and loosely corresponds to the roughness Reynolds number referred to in §1. Figure 10 displays amplification curves for various values of Re_s as a function of Re for the wall suction with the wavenumber $\alpha = 1.8$. This wavenumber gives rise to the (approximately) most rapidly amplified vortices, according to figures 6 and 7. It can be seen that for small enough Re, the disturbances are stable regardless of the value of Re_s. The character of the changes of the amplification rates with an increase of Re depends on the magnitude of Re_s. In the case of $Re_s > 14$, when Re increases above a certain critical value (whose magnitude depends on Re_s), the changes of amplification are non-monotonic, i.e. there is at first a rapid increase followed by a decrease. However, when $Re_s < 14$, there is only a gradual (monotonic) increase of the amplification. For values of Re large enough (approximately larger than 4000), the amplification rates approach a constant asymptotic value whose magnitude depends on Re_s. This happens regardless of a particular value of Re_s. The asymptotic value of the amplification does not become positive (in the range of parameters studied, i.e. for $Re < 10\,000$) if $Re_s < 10$. It can be concluded, on the basis of these results, that the wall suction does not destabilize the flow (in the range of parameters studied) when $Re_s < 10$. Under such conditions, surface flow modifications due to the wall suction are completely negligible and we can refer to the wall as being equivaent to a 'hydraulically smooth wall'.

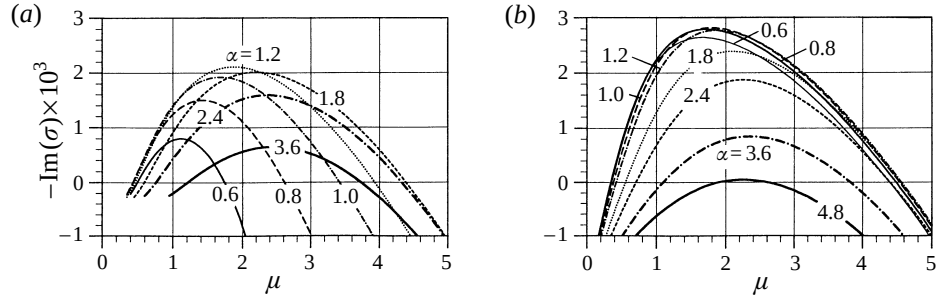

FIGURE 11. Amplification rate $-\mathrm{Im}(\sigma)$ as a function of the spanwise wavenumber μ for the Poiseuille flow with $Re = 5000$. The flow is modified by wall suction in the form (4.1) with $\phi = 0$, $S = 0.004$. (*a*) $S_u = 0$; (*b*) $S_u = -0.004$. The case of $S_u = 0.004$ is shown in figure 7(*a*).

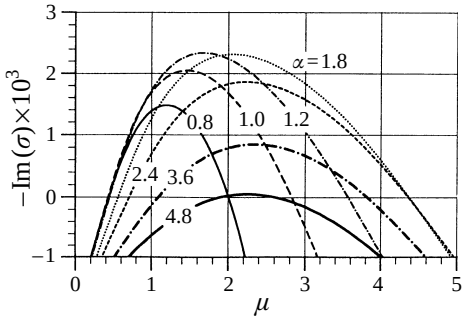

FIGURE 12. Amplification rate $-\mathrm{Im}(\sigma)$ as a function of the spanwise wavenumber μ for the Poiseuille flow with $Re = 5000$. The flow is modified by wall suction in the form (4.1) with $S = S_u = 0.004$ and $\phi = \frac{1}{2}\pi$. *Note*: (i) stability diagram for $\phi = \frac{3}{2}\pi$ is identical to that for $\phi = \frac{1}{2}\pi$ owing to invariance under transformation $x \to -x$; (ii) case $\phi = \pi$ is identical as for $S = -S_u = 0.004$, $\phi = 0$ (figure 11*b*); (iii) case $\phi = 0$ is shown in figure 7(*a*).

4.2. *Poiseuille flow with other forms of suction*

In this section, we shall inquire how a change in the configuration of the wall suction affects the stability properties of the complete flow. The simplest model problem consists of a suction with different amplitudes at both walls and a phase shift between them. The boundary conditions in the form (2.3) are replaced by

$$v_1(x, z, -1) = \tfrac{1}{2}S\,\mathrm{e}^{\mathrm{i}\alpha x} + \mathrm{c.c.}, \quad v_1(x, z, +1) = \tfrac{1}{2}S_u\,\mathrm{e}^{\mathrm{i}(\alpha x+\phi)} + \mathrm{c.c.} \qquad (4.1\,a, b)$$

where S, S_u are real and denote the amplitude of the suction at the lower and upper walls, respectively, and ϕ describes a phase shift of the suction at the upper wall with respect to the suction at the lower wall. The corresponding flow modifications are determined using the method described in §2. The linear stability analysis is carried out as described in §3. Details of these analyses are omitted.

Results shown in figure 11 illustrate the effects of variations of the amplitude of the suction at the upper wall S_u while keeping the amplitude of the suction at the lower wall S constant. It can be seen that for $S_u \in [-S, S]$ the instability process is qualitatively unchanged, although the numerical values of the amplification rates are subject to some variations. The dominant mode corresponds to $m = 0$, $\delta = 0$ and $\mathrm{Re}(\sigma) = 0$ in (3.9).

Effects of the phase shift ϕ are illustrated in figure 12 for $\phi = 0$, $\frac{1}{2}\pi$, π, $\frac{3}{2}\pi$ with $S = S_u = 0.004$. Again, it can be seen that while the amplification rates change somewhat as a function of ϕ, the instability remains qualitatively unchanged.

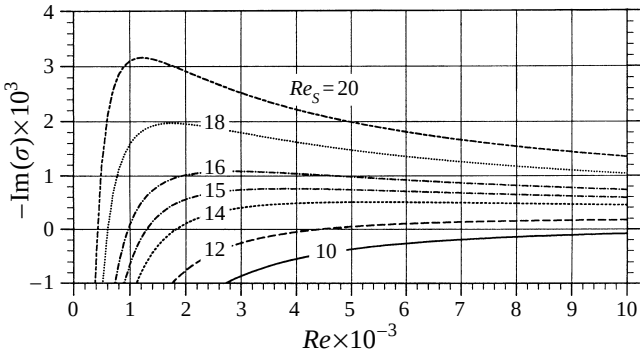

FIGURE 13. Amplification rate $-\mathrm{Im}(\sigma)$ as a function of the Reynolds number Re for various values of the suction Reynolds number Re_s for the Poiseuille flow modified by suction in the form (4.1) with $\phi = 0$, $S_u = 0$, $\alpha = 1.8$, $\mu = 2.0$.

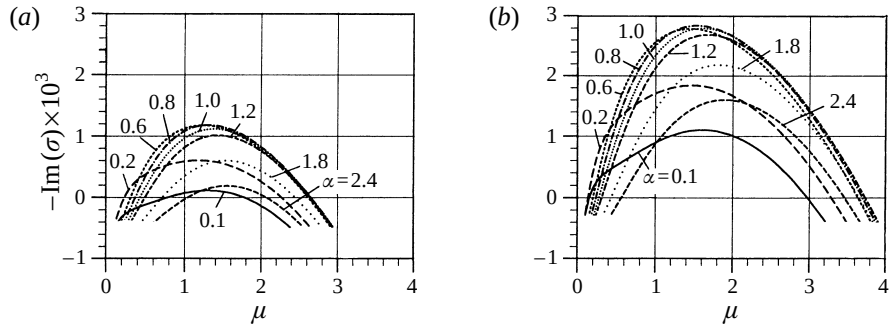

FIGURE 14. Amplification rate $-\mathrm{Im}(\sigma)$ as a function of the spanwise wavenumber μ for the Couette flow with $Re = 3000$. The flow is modified by wall suction in the form (4.1*a*). (*a*) $S = 0.004$; (*b*) $S = 0.006$.

Figure 13 displays amplification rates as a function of Re for various values of the suction Reynolds number Re_s, defined in the same way as in the previous section, with the amplitude of the suction at upper wall $S_u = 0$. Comparison with figure 10 demonstrates a very close similarity of the instability process for these two cases. As before, $Re_s < 10$ guarantees that the wall suction does not induce any instability.

The results discussed above show that, in the range of parameters studied, (fundamentally) the same instability process is induced by various configurations of the wall suction

4.3. *Couette flow*

It is of interest to investigate how other shear layers may be affected by the same wall suction as used in the case of the Poiseuille flow. A good test case is provided by the Couette flow induced by motion of the upper wall. The reader may recall that this flow is linearly stable. The velocity distribution has the form $u_0(y) = \frac{1}{2}(y+1)$, where the velocity of the upper wall and the half channel height have been used as the velocity and the lengthscales, respectively. The flow is modified by introducing suction in the form (4.1*a*), i.e. only at the lower (stationary) wall. Flow modifications and stability characteristics are determined following the theory described in §§2 and 3. Details of the analysis are omitted.

Results displayed in figures 14 and 15 demonstrate that the surface suction is able to destabilize the flow. The disturbances have the form of streamwise vortices, as in the

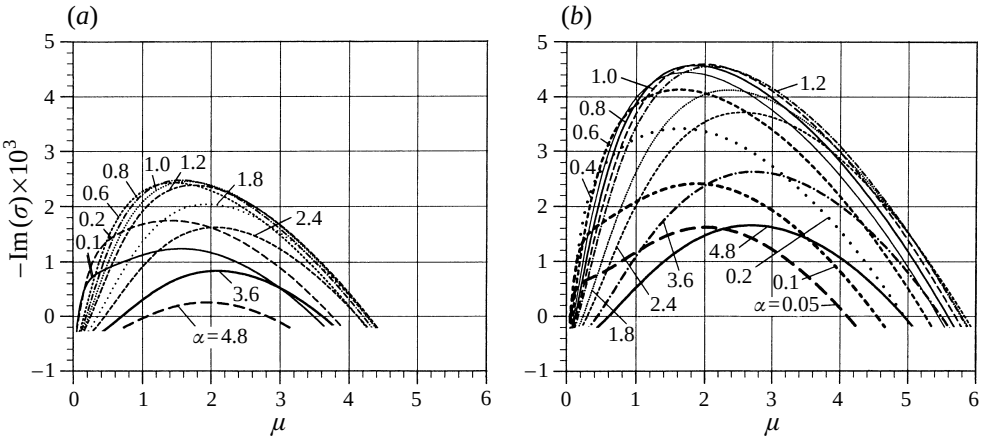

FIGURE 15. Same as in figure 14. $Re = 5000$. (*a*) $S = 0.004$; (*b*) $S = 0.006$.

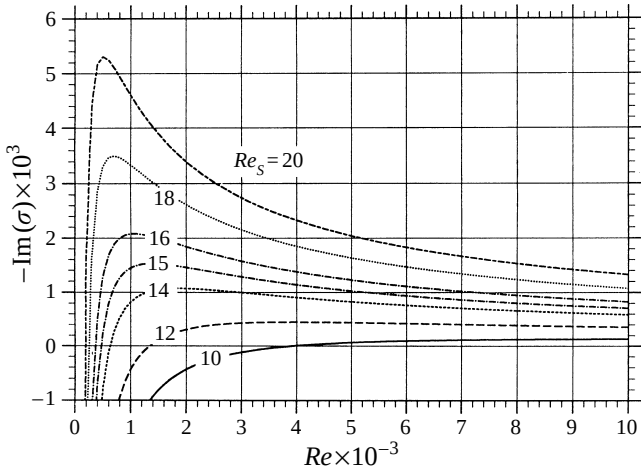

FIGURE 16. Amplification rate $-\mathrm{Im}(\sigma)$ as a function of the Reynolds number Re for various values of the suction Reynolds number Re_s for the Couette flow modified by wall suction in the form (4.1*a*) with $\alpha = 1.8$, $\mu = 2.0$.

case of the Poiseuille flow, i.e. the dominant mode corresponds to $m = 0$, $\delta = 0$ and $\mathrm{Re}(\sigma) = 0$ in (3.9). The amplification rates and the bandwidth of the unstable spanwise wavenumbers μ increase with an increase of both the suction amplitude S and the Reynolds number Re. Disturbances with $\mu \approx 1.5$ appear to have the largest amplification rates. The suction with the wavenumber $\alpha \approx 0.8$ appears to be the most dangerous in the sense that it induces disturbances with the highest amplification rates. The stability diagrams are qualitatively very similar to those obtained in the case of the Poiseuille flow (compare with figures 6 and 7). The only significant difference (if one disregards different numerical values of the amplification rates) is that the Couette flow can be destabilized by suction with a fairly long wavelength (even with $\alpha = 0.1$), while for the Poiseuille flow, α had to be larger than 0.6 in the range of parameters studied. Also, the most destabilizing suction corresponds to $\alpha \approx 0.8$ compared to $\alpha \approx 1.8$ in the Poiseuille flow case.

Figure 16 displays amplification rates as a function of Re for various values of the

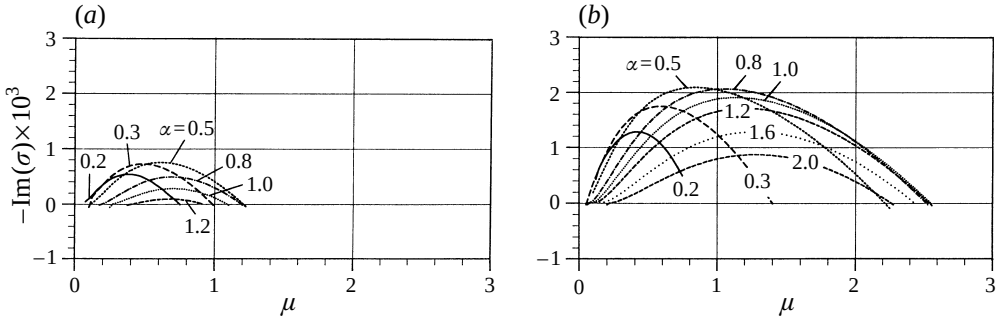

FIGURE 17. Amplification rate $-\mathrm{Im}(\sigma)$ as a function of the spanwise wavenumber μ for the Blasius boundary layer modified by wall suction in the form (4.2) with $S = 0.006$. (*a*) $Re = 1000$; (*b*) $Re = 2000$.

suction Reynolds number Re_s defined as in the previous section. Comparison with the Poiseuille flow (see figures 10 and 13) demonstrates a very close similarity of the instability process in all cases. The wall suction does not induce any instability for Re_s slightly smaller than 10 in the range of parameters studied.

Results discussed above show that the instability process is qualitatively very similar for both types of shear layers. In the next section, we shall consider the third type of shear layer, i.e. the Blasius boundary layer.

4.4. *Blasius boundary layer*

The flow field is scaled using the velocity at the edge of the boundary layer and the displacement thickness as the velocity and the lengthscales, respectively. The reader may recall that this boundary layer becomes linearly unstable at $Re \approx 520$ in the case of an ideal wall and parallel flow approximation. In this analysis, we also assume the flow to be parallel and impose periodic suction at the wall. The relevant boundary conditions have the form

$$u_1(x,z,0) = 0, \quad v_1(x,z,0) = \tfrac{1}{2}S\mathrm{e}^{\mathrm{i}\alpha x} + \mathrm{c.c.} \tag{4.2a}$$

$$u_1(x,z,y) \to 0, \quad v_1(x,y,z) \to 0 \quad \text{as} \quad y \to \infty, \tag{4.2b}$$

where the latter expresses disappearance of flow modifications owing to the wall suction at large distances away from the wall. For computational purposes the half-infinite domain $y \in [0,\infty]$ is mapped onto a strip $Y \in [0,1]$ using transformation $Y = \exp(-y/y_0)$ with $y_0 \approx 5$ used typically in the computations. The transformed equations were discretized by employing a spectral collocation method based on Chebyshev polynomials. Details of the solution procedure are omitted (see, for example, Casalis 1989). The linear stability analysis is similar to the one described in §3. The relevant boundary conditions correspond to the disappearance of disturbances at the wall and far away from the wall. For computational purposes, the half-infinite solution domain for the disturbance equations is mapped onto a finite strip using the same exponential transformation as discussed above. The transformed disturbance equations were discretized using the same spectral collocation method. Details of the solution procedure are omitted.

Results displayed in figure 17 demonstrate that the surface suction is able to induce a new class of disturbances, i.e. streamwise vortices, similar to the case of the Poiseuille and Couette flows. The dominant mode corresponds to $m = 0$, $\delta = 0$ and $\mathrm{Re}(\sigma) = 0$ in

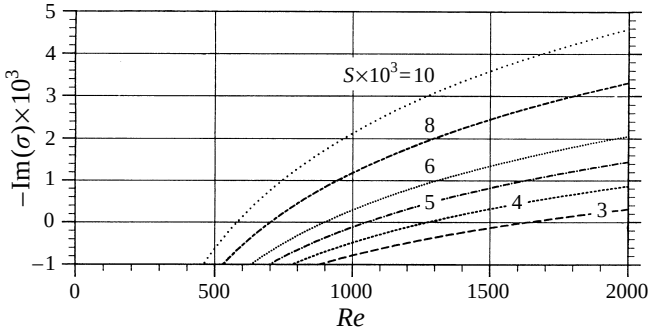

FIGURE 18. Amplification rate $-\mathrm{Im}(\sigma)$ as a function of the Reynolds number Re in the case of the Blasius boundary layer modified by wall suction in the form (4.2) with $\alpha = 0.8$, $\mu = 1.0$ and various values of the suction amplitude S.

(3.9). Such disturbances are responsible for rapid three-dimensionalization of the flow field. The form of the curves of constant amplification shown in figure 17 for $Re = 1000$ and 2000 with $S = 0.006$ is qualitatively similar to those obtained in the case of shear layers described in the previous sections. The amplification and the bandwidth of the unstable spanwise wavenumbers μ increase with an increase of the suction amplitude S and the Reynolds number Re. However, unlike the previous cases, the maximum amplification shifts from disturbances with $\mu \approx 0.5$ at $Re = 1000$ to $\mu \approx 1.0$ at $Re = 2000$. Wall suction with $\alpha \approx 0.5$ appears to be the most dangerous in the sense that it induces disturbances with the highest amplification.

Variations of the amplification rates as a function of Re for the suction-induced-disturbances are illustrated in figure 18. The amplification rates are of the same order of magnitude as those for the unstable TS-waves and they increase with an increase of S and Re. The results demonstrate that the suction may induce instability at Re smaller than the one required to induce the TS-waves if the suction amplitude $S > 10^{-2}$. This points to the phenomenon of boundary-layer tripping in the case of a real roughness, if the roughness amplitude is large enough.

Suction amplitudes smaller than 10^{-2} induce instability at higher values of Re than that required to induce the TS-waves. This, however, should not be interpreted as a proof that such a weak suction becomes unimportant in the laminar–turbulent transition process. The reader may note that while the TS-waves begin to grow earlier, i.e. closer to the leading edge, they have a two-dimensional character and rather small growth rates. The streamwise vortices, however, unlike the TS-waves, rearrange the flow field qualitatively (three-dimensionalize it). This process involves lifting the low-momentum fluid away from the wall and thus creating high in-flow shear layers that are subject to very strong secondary instabilities (Yu & Liu 1991). This may initiate a (bypass) transition process with qualitatively different dynamics than the one induced by the TS-waves and this process may quickly overcome the one driven by the TS-waves forcing the flow to go through a potentially much faster (bypass) route to transition.

Figure 19 displays amplification rates of the suction-induced-disturbances as a function of Re for several values of the suction Reynolds number Re_s defined as in the previous sections. These curves have a qualitatively similar character to the corresponding curves for the Poiseuille and Couette flows (see figures 10, 13 and 16). One can observe that the disturbances are not amplified if $Re_s < 5$ (in the range of parameters studied). In the case of $Re_s > 7$, the disturbances are amplified more at

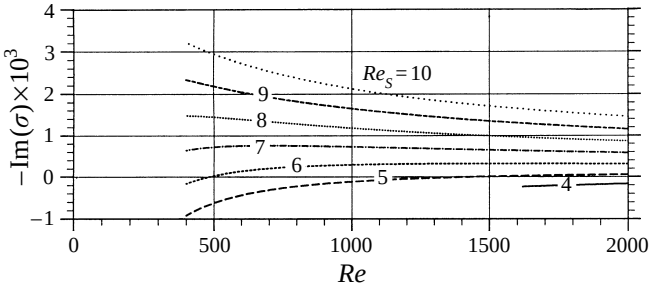

FIGURE 19. Amplification rate $-\mathrm{Im}(\sigma)$ as a function of the Reynolds number Re in the case of the Blasius boundary layer modified by wall suction in the form (4.2) with $\alpha = 0.8$, $\mu = 1.0$ and various values of the suction Reynolds number Re_s.

smaller values of Re, which points to the higher sensitivity of boundary layers close to the leading edge to surface modifications, if the amplitude of such modifications is larger than a certain critical value.

5. Summary

Stability of wall-bounded shear layers modified by distributed wall suction has been considered. Wall suction was introduced in order to simulate distributed surface roughness. The analysis focused on the suction in the form of a single two-dimensional Fourier mode and consisted of two steps, i.e. (i) determination of the new suction-modified flow, followed by (ii) a linear stability analysis of this flow.

Explicit calculations carried out in the case of a plane Poiseuille flow showed that the flow modifications due to the presence of suction can be described by a linear model if the suction amplitude $S < 10^{-2}$. Under such conditions, flow modifications due to an arbitrary suction can be determined using a combination of Fourier decomposition of the suction distribution, mode-by-mode analysis and linear superposition.

Linear stability calculations have been carried out for three types of flow, i.e. plane Poiseuille flow, plane Couette flow and Blasius boundary layer. In all cases, wall suction was able to induce a new type of instability characterized by the appearance of streamwise vortices as the dominant mode. The instability occurred only if the suction amplitude S reached a certain critical value. In all cases, $S < 10^{-2}$ was sufficient to induce the instability. Explicit calculations carried out in the case of Poiseuille flow showed that the nonlinear distortion of the mean flow owing to the presence of surface suction had no effect on the linear stability characteristics (for the magnitude of suction amplitudes considered). One may conclude that the linear model of suction-induced flow modifications is sufficient for analysis of the stability of the flow. This means that it is sufficient to carry out stability analysis on the mode-by-mode basis once and for ever rather than studying each particular suction distribution on a case-by-case basis. Given a particular suction distribution, its stability properties can be assessed by simply identifying the Fourier components present. Stability diagrams for the Fourier modes that give rise to the instability are presented in this paper.

An increase of the suction amplitude S results in reduction of the critical Reynolds number for all flows studied. The strength of the instability, as measured by disturbance amplification rates, increases almost linearly with S. The dominant mode has the form of streamwise stationary vortices. A whole band of spanwise wavenumbers is amplified and the width of this band increases with S and Re. The most amplified spanwise wavenumber corresponds to $\mu \approx 2.0$ for the Poiseuille flow, $\mu \approx 1.5$ for the

Couette flow and $\mu \in (0.5, 1.0)$ for the Blasius boundary layer. The most dangerous mode in the suction distribution, in the sense that it induces the most amplified disturbances, corresponds to the wavenumber $\alpha \approx 1.8$ for the Poiseuille flow, $\alpha \approx 0.8$ for the Couette flow and $\alpha \approx 0.5$ for the Blasius boundary layer. In all three cases, the classical Tollmien–Schlichting waves were found to be little affected by the suction levels considered.

The available results point to the existence of a generic instability mechanism based on a parametric resonance and related to the suction-induced spatial periodicity of the flow. The mechanism can be activated regardless of any particular form of shear layer, as documented by the results from three case studies (i.e. Poiseuille flow, Couette flow and Blasius boundary layer) discussed in this paper. Explicit results in the case of Poiseuille flow show that the mechanism is also independent of any particular configuration of suction, as long as the same periodicity of the flow is maintained. It is expected that the presence of a real (rather than simulated) roughness will lead to a similar flow response owing to the appearance of a spatial periodicity of the roughness-modified flow.

Appearance of streamwise vortices results in a significant rearrangement and a rapid three-dimensionalization of the flow. Uplifting of low-momentum fluid away from the wall leads to the formation of highly distorted streamwise and spanwise velocity profiles that are functions of streamwise and spanwise coordinates and are subject to very strong secondary instabilities. It has been shown by direct numerical simulations (Floryan *et al.* 1992) that the suction-induced instability identified here leads to a new (bypass) route to transition.

Since the presence of streamwise vortices is a strong harbinger of transition to turbulence, one is interested in determining the maximum suction amplitude that the flow can accommodate without inducing such vortices. The available results show that it is possible to formulate the relevant criteria using suction Reynolds number Re_s. The instability does not occur if $Re_s < 10$ in the case of Poiseuille and Couette flows (for $Re < 10\,000$) and $Re_s < 5$ for the Blasius boundary layer (with $Re < 2000$); the walls with such a suction are equivalent to 'hydraulically smooth' walls.

The author would like to thank Drs K. Yamamoto, D. Arnal and G. Casalis for discussions on the subject of this paper. The stability calculations have been carried out using a code originally written by Dr G. Casalis. Computer time has been provided by CERT/ONERA, Toulouse, France. The author would like to thank E. Montreuil for his assistance in carrying out computations.

REFERENCES

Casalis, G. 1989 Resolution de l'equation d'Orr–Sommerfeld en tridimensionnel et en incompressible par une methode de Galerkin avec les polynomes de Chebichev. *Rapport Technique No.* 46/5618.34. Dept d'Aerothermodynamique, CERT/ONERA, Toulouse, France.

Casalis, G. 1991 Instabilité secondaire de la couche limite laminaire tridimensionnelle en écoulement incompressible: description du code de calcul. *Rapport Technique No.* 63/5618.54. Dept d'Aerothermodynamique, CERT/ONERA, Toulouse, France.

Coddington, E. A. & Levinson, N. 1965 *Theory of Ordinary Differential Equations*. McGraw-Hill.

Corke, T. C., Bar Sever, A. & Morkovin, M. V. 1986 Experiments on transition enhancement by distributed roughness. *Phys. Fluids* **29**, 3199–3213.

De Anna, R. G. 1993 Direct numerical simulation of instabilities of parallel flow with spherical roughness elements. In *Instabilities and Turbulence in Engineering Flows* (ed. B. E. Ashpis, T. B. Gatski & R. Hirsh), pp. 95–128, Kluwer.

DOENHOFF, A. E. VON, & BRASLOW, A. L. 1961 The effect of distributed surface roughness on laminar flow. In *Boundary Layer and Flow Control* (ed. G. V. Lachmann), vol. 2, pp. 657–681. Pergamon.

FEINDT, E. G. 1957 Untersuchungen über die Abhängigkeit des Umschlages laminar–turbulent von der Oberflächenraukigkeit und der Druckverteilung. *Jahrbuch 1956 der Schiffbautechnischen*, Gesellschaft 50, pp. 180–203.

FLORYAN, J. M. 1990 On the modelling of roughness effects. In *Instability and Transition* (ed. M. Y. Hussaini & R. G. Voigt) vol. 2, pp. 258–267. ICASE/NASA LARC Series, Springer.

FLORYAN, J. M. 1993 On the effects of surface roughness on the laminar–turbulent transition process. In *Proc. First Bombardier International Workshop, 20–21 Sept. 1993*. École Polytechnique de Montreal, Montreal, Canada, pp. 346–365.

FLORYAN, J. M. & DALLMANN, U. 1990 Flow over a leading edge with distributed roughness. *J Fluid Mech.* **216**, 629–656.

FLORYAN, J. M., YAMAMOTO, K. & MURASE, T. 1992 Laminar–turbulent transition process in the presence of simulated wall roughness. *Can. Aeronaut. & Space J.* **38**, 173–182.

HERBERT, T. 1977 Finite amplitude stability of plane parallel flows. *AGARD Conf. Proc.* **224**, 3.1–3.10.

HERBERT, T. 1988 Secondary instability of boundary layers. *Ann. Rev. Fluid Mech.* **20**, 487–526.

KENDALL, J. M. 1981 Laminar boundary layer velocity distortion by surface roughness, effect upon stability. *AIAA Paper* 81-0195.

LESSEN, M. & GANGWANI, S. T. 1976 Effect of small amplitude wall waviness upon the stability of the laminar boundary layer. *Phys. Fluids* **19**, 510–513.

MORKOVIN, M. V. 1990 On roughness-induced transition: facts, views and speculations. In *Instability and Transition* (ed. M. Y. Hussaini & R. G. Voigt), vol. 1, pp. 281–295. ICASE/NASA LARC Series, Springer.

ORSZAG, S. A. 1971 Accurate solutions of the Orr–Sommerfeld stability equation. *J. Fluid Mech.* **50**, 689–704.

PEREYRA, V. 1979 PASVA 3: An adaptive finite-difference Fortran program for first order nonlinear boundary value problems. In *Codes for Boundary-Value Problems in Ordinary Differential Equations*. Lecture Notes in Computer Science, vol. 76, p. 67. Springer.

RESHOTKO, E. 1984 Disturbances in a laminar boundary layer due to distributed surface roughness. In *Turbulence and Chaotic Phenomena* (ed. T. Tatsumi). Proceedings of IUTAM Symposium, pp. 39–46. Elsevier.

RESHOTKO, E. & LEVENTHAL, L. 1981 Preliminary experimental study of disturbances in a laminar boundary layer due to distributed surface roughness. *AIAA Paper* 81-1224.

SCHLICHTING, H. 1979 *Boundary Layer Theory*, 7th edn. McGraw-Hill.

SINGH, K. & LUMLEY, J. L. 1971 Effect of roughness on the velocity in a laminar boundary layer. *Appl. Sci. Res.* **24**, 168–186.

TADJFAR, M., RESHOTKO, E., DYBBS, A. & EDWARDS, R. V. 1985 Velocity measurements within boundary layer roughness using index matching. *Intl Symp. on Laser Anemometry* (ed. A. Dybbs & P. A. Pfund). FED vol. 33, ASME, pp. 59–73.

TANI, I. 1971 Effect of two dimensional and isolated roughness elements. In *Boundary Layer and Flow Control* (ed. G. V. Lachmann), vol. 2, pp. 637–656. Pergamon.

YU, X. & LIU, J. T. C. 1991 The secondary instability of Görtler flow. *Phys. Fluids* A **3**, 1845–1847.